



Isotropic distributions in hcp crystals

Grażyna Kontrym-Sznajd

Abstract. Some anisotropic quantities in crystalline solids can be determined from their knowledge along a limited number of sampling directions. The importance of the choice of such directions is illustrated on the example of estimating, from angular correlation of annihilation radiation data, the isotropic electron momentum density in Gd.

Key words: Brillouin zone • lattice harmonics • special directions • isotropic distribution

This paper is devoted to the studies of the isotropic average of quantities in the momentum space having the full symmetry of the Brillouin zone. Such quantities, denoted here as $f(\mathbf{p})$, can be expressed as a series of lattice harmonics $F_{l,\nu}(\theta, \phi)$ of an appropriate symmetry [1, 2]

$$(1) \quad f(\mathbf{p}) = \sum_{l,\nu} f_{l,\nu}(p) F_{l,\nu}(\Theta, \phi)$$

where ν distinguishes harmonics of the same order and (Θ, ϕ) are the azimuthal and polar angles of the direction \mathbf{p} with respect to the reciprocal lattice coordinate system.

Isotropic distributions $f_0(p)$ ($f(\mathbf{p})$ averaged over angles (Θ, ϕ)) are used in calculating many physical properties, e.g. the specific heat and Debye temperature [1, 3–7] and density of states in disorder systems [8, 9], or (in some particular cases) in probing electron momentum densities via angular correlation of annihilation radiation (ACAR) [10, 11], Compton scattering [12–22], and Doppler broadening spectra [23].

In the previous paper, devoted to the cubic structures [24], we showed that for calculating the isotropic component, the common procedure of applying high symmetry directions (HSD) is the worst choice (the same occurs for the anisotropic components). In this paper, similar considerations are performed for the hcp structure, although obtained results may be generalized on all structures with the unique R -fold axes. For such structures with $R = 6, 4$, and 3 (hcp, tetragonal, and trigonal symmetry, respectively), the lattice harmonics having the full symmetry of the Brillouin zone have a very simple form:

G. Kontrym-Sznajd
W. Trzebiatowski Institute of Low Temperature
and Structure Research, Polish Academy of Sciences,
P. O. Box 1410, 50-950 Wrocław 2, Poland,
E-mail: g.sznajd@int.pan.wroc.pl

Received: 18 June 2015
Accepted: 20 August 2015

$$(1a) \quad F_{l,m} = \begin{cases} a_l P_l(\cos \Theta), & l = 2 \cdot i \text{ and } i = 0, 1, 2, \dots \\ a_{l,m} P_l^{(m)}(\cos \Theta) \cos(m\phi), & l = R + 2 \cdot i \\ & \text{and } m = R + Ri \text{ where } m \leq l \end{cases}$$

where $P_l^{(m)}$ are associated Legendre polynomials and a are the normalization constants.

In Ref. [23], the isotropic $f_0(p)$ for the hcp Co and Gd was estimated based on 3-HSD ([10 $\bar{1}$ 0], [11 $\bar{2}$ 0], and [0001]). Because, in the hcp lattice, the first harmonic, which distinguishes directions [10 $\bar{1}$ 0] and [11 $\bar{2}$ 0], is the fifth harmonic $F_{6,6}$, $f_0(p)$ can be estimated either as the average

$$(2) \quad f_0^a(p) = [f_{[10\bar{1}0]}(p) + f_{[11\bar{2}0]}(p) + f_{[0001]}(p)] / 3$$

or as

$$(3) \quad f_0^a(p) = 0.380952f_{[10\bar{1}0]}(p) + 0.380952f_{[11\bar{2}0]}(p) + 0.238095f_{[0001]}(p)$$

where the symbol 'a' denotes approximated function.

Equations (2) and (3) correspond to the use, respectively, of first ($l = 0$), second ($l = 2$), fifth ($l = 6$, $m = 6$) and first ($l = 0$), fourth ($l = 6$), fifth ($l = 6$, $m = 6$) harmonics. The quality of each approximation can be estimated via d coefficients, which define a deviation of $f_{l,v}^a(p)$ from its true value $f_{l,v}(p)$ (see Eq. (4) in Ref. [24]). In this way, one can show that none of the Eqs. (2) and (3) is favorable, which is connected with the fact that harmonics along HSD (first of all along [0001]) have very high values – hence, corresponding values of d coefficients are also high.

In Figs. 1 and 2, we present $\Delta f_0(p) = f_0(p) - f_0^a(p)$ estimated for one-dimensional (1D) ACAR spectra for Gd, created from two-dimensional (2D) ACAR experimental data [25]. Gd was chosen for two reasons: (1) the ineffective approach in Ref. [23] was applied for Gd; (2) having at disposal sixteen 2D ACAR spectra [25], it was possible to determine, with high accuracy, each quantity connected with both 1D and 2D ACAR spectra, so also fully isotropic $f_0(p)$.

$f_0^a(p)$ calculated using Eqs. (2) and (3) are compared with $f_0^a(p)$ estimated for only two but special directions (SDs)

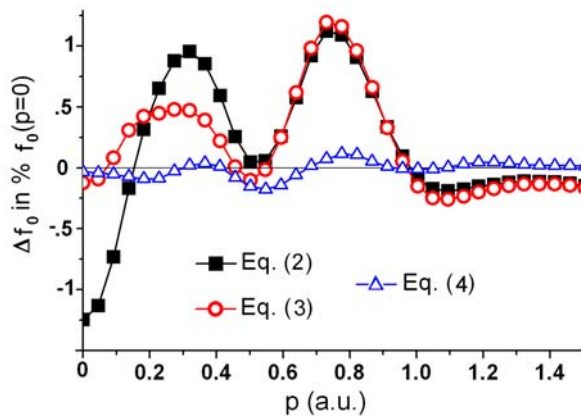


Fig. 1. $\Delta f_0(p) = f_0(p) - f_0^a(p)$ estimated for 3-HSD (Eqs. (2) and (3)) and 2-SDs (Eq. (4)). All quantities were constructed using 16 experimental 2D ACAR data for Gd [25].

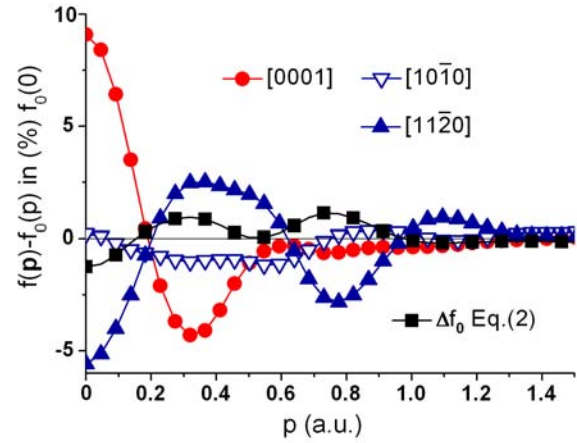


Fig. 2. Anisotropy of 1D ACAR spectra for Gd, compared with $\Delta f_0(p)$ obtained from Eq. (2).

$$(4) \quad f_0^a(p) = 0.347855f(p, \Theta_1, \phi = 15^\circ) + 0.652145f(p, \Theta_2, \phi = 15^\circ)$$

determined by two positive zeros ($\Theta_1 = 30.5556^\circ$ and $\Theta_2 = 70.1243^\circ$) of $P_4(\cos \Theta)$, first harmonic omitted in Eq. (1).

In Gd, the highest values of anisotropic components $f_{l,v}(p)$ are achieved by $f_{6,0}(p)$ and $f_{6,6}(p)$ – see Fig. 1 of Ref. [26]. The fact that they are greater than those of lower degree (with $l = 2$ and 4) is not unusual – it depends on a particular lattice potential: either anisotropy dominates on the planes perpendicular to the main rotation axis (as in Gd or Y [27]) or along the main rotation axis (as, e.g., in Cd [28], where the largest is $f_2(p)$). Because harmonics $f_{l,0}$ along the [0001] direction have very high values, growing with l , anisotropy of 1D profiles could be very high compared to absolute values of particular anisotropic components $f_{l,v}(p)$.

Absolute values of $\Delta f_0(p)$, estimated for experimental ACAR data for Gd, are of the order of $f_{6,0}(p)$, far exceeding values of other $f_{l,v}(p)$, which are necessary to be taken into account if one wants to reproduce the anisotropy displayed in Fig. 2 (compare it with Fig. 1 in [26]). Moreover, a deviation of $f_0^a(p)$ from the true $f_0(p)$ is well seen on the corresponding average of 3D density, determined from the Stewart's relation [29] $\rho_0(p) = \{-1/p \cdot [(df_0(p)/dp)]\}$ (see Fig. 3, where to avoid a singularity in the expression on $\rho_0(p)$, $f_0(p)$ was expanded into a series of even the Chebyshev polynomials of the second kind).

Thus, in view of anisotropy, $\Delta f_0(p)$ has noticeable values the more so as (1) used 2D ACAR spectra was smeared by both the experimental resolution (FWHM = 0.12 a.u.) and electron-electron correlations; (2) creating 1D spectra from 2D data (via integrating procedure) introduces additional smearing; and (3) results are in percentage of $f_0(0)$, which contains both valence and core electrons (the contribution of core is significantly reduced by the presence of the positron but, nevertheless, it is noticeable). Moreover, positrons mostly reduce the higher momentum components of the electron densities, i.e. it decreases the anisotropy). All these indicate that for valence electrons, absolute values

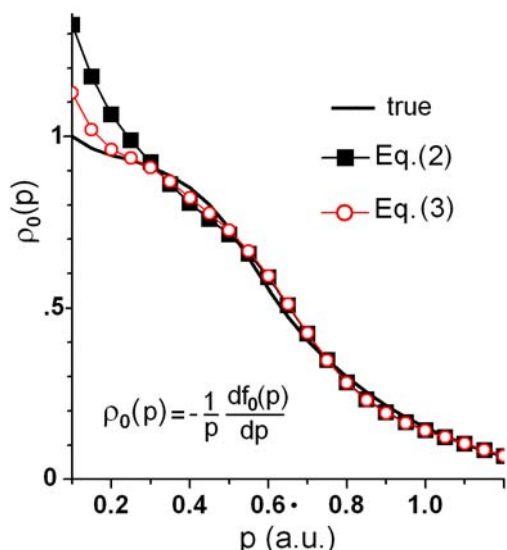


Fig. 3. The average of three-dimensional density, $\rho_0(p)$, for true and two approximated functions $f_0(p)$.

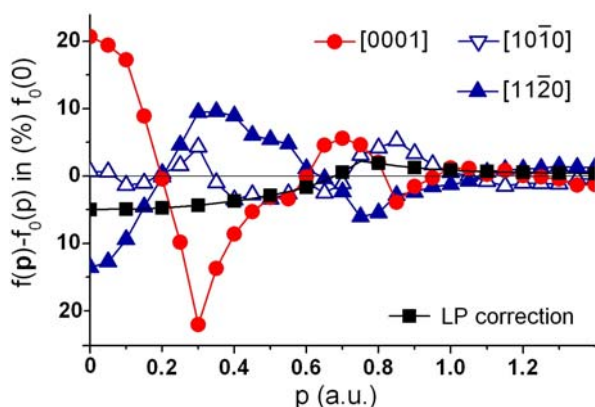


Fig. 4. Anisotropy of theoretical Compton scattering spectra and the LPC for valence electrons in Y (theoretical data are not convoluted to simulate a finite resolution of an experimental spectrometer).

of anisotropic components $f_{i,v}(p)$ (hence, also $\Delta f_0(p)$) will be much higher.

Anisotropic components of experimental 1D ACAR spectra for Gd are almost identical with those for Y (both their shape and values). Thus, in order to visualize the importance of a proper determining of $f_0(p)$, first of all when one performs theoretical calculations, in Fig. 4, we show the anisotropy of theoretical spectra in Y [27] compared with Lam-Platzman correction (LPC), which describes electron-electron correlation effects [30].

A comparison with the results displayed in Fig. 2 clearly reveals that in Gd and Y, inaccuracy of determining the isotropic component f_0 , based on 3-HSD, is of the order of the LPC. Meanwhile, very often does one determine f_0 to examine the correctness of this correction [30], i.e. to study much more subtle effects [31].

Additionally, a comparison of results presented in Figs. 4 and 2 shows how much a resolution function of the equipment smoothes anisotropy. Therefore, in the case of Doppler spectra, as in Ref. [23], the approximations (2) or (3) are able to describe

the isotropic component. It is not the case for high-resolution Compton profiles, while for theoretical calculations, such approximations are unacceptable – for them, all quantities shown in Fig. 1 would be about two times larger.

Conclusions

We showed (here for the hcp, previously for the cubic structures) that a traditional way of calculating the isotropic average using HSD yields incomparably worse results than applying SDs [32–35]. The huge number of papers in which HSD are used to determine the average distributions (here only a part of such papers was quoted) prove the importance of the problem, which is worth more attention.

References

- Houston, W. V. (1948). Normal vibrations of a crystal lattice. *Rev. Mod. Phys.*, 20, 161–165.
- Mueller, F. M., & Priestley, M. G. (1966). Inversion of cubic de Haas-van Alphen Data, with an application to palladium. *Phys. Rev.*, 148, 638–643.
- Bhatia, A. B. (1955). Vibration spectra and specific heats of cubic metals. I. Theory and application to sodium. *Phys. Rev.*, 97, 363–371.
- Betts, D. D., Bhatia, A. B., & Womann, M. (1956). Houston's method and its application to the calculation of characteristic temperatures of cubic crystals. *Phys. Rev.*, 104, 37–42.
- Betts, D. D., Bhatia, A. B., & Horton, J. W. (1956). Debye characteristic temperatures of certain noncubic crystals. *Phys. Rev.*, 104, 43–47.
- Ghosh, G., Delsante, S., Borzone, G., Asta, M., & Ferro, R. (2006). Phase stability and cohesive properties of Ti-Zn intermetallics: First-principles calculations and experimental results. *Acta Mater.*, 54, 4977–4997.
- Taylor, C. D., Lookman, T., & Scott, L. R. (2010). Ab initio calculations of the uranium-hydrogen system: Thermodynamics, hydrogen saturation of a-U and phase-transformation to UH₃. *Acta Mater.*, 58, 1045–1055.
- Bansil, A. (1979). Coherent-potential and average-matrix approximations for disordered muffin-tin alloys. II. Application to realistic systems. *Phys. Rev. B*, 20, 4035–4043.
- Prasad, R., & Bansil, A. (1980). Special directions for Brillouin-zone integration: Application to density of states calculations. *Phys. Rev. B*, 21, 496–503.
- Šob, M., Szuszkiewicz, S., & Szuszkiewicz, M. (1984). Polarized positron annihilation enhancement effects in ferromagnetic iron. *Phys. Status Solidi B*, 123, 649–652.
- Šob, M. (1985). Electronic structure and positron annihilation in alkali metals: Isolation of ionic core contribution and valence high-momentum components. *Solid State Commun.*, 53, 249–253.
- Aguiar, J. C., Mitnik, D., & DiRocco, H. O. (2015). Electron momentum density and Compton profile by a semi-empirical approach. *J. Phys. Chem. Solids*, 83, 64–69.
- Ahuja, B. L., Sharma, M. D., Sharma, B. K., Hamouda, S., & Cooper, M. J. (1994). Compton profile of polycrystalline yttrium. *Phys. Scripta*, 50, 301–304.

14. Ahuja, B. L., Sharma, M., & Bross, H. (2007). Compton profile study of gold: Theory and experiment. *Phys. Status Solidi B*, 244, 642–649.
15. Ahuja, B. L., Mohammad, F. M., Mohammed, S. F., Sahariya, J., Mund, H. S., & Heda, N. L. (2015). Compton scattering and charge transfer in Er substituted DyAl₂. *J. Phys. Chem.*, 77, 50–55.
16. Bross, H. (2006). Special directions for surface integrals in cubic lattices with application to the evaluation of the Compton profile of copper. *Phys. Status Solidi B*, 243, 653–665.
17. Bross, H. (2004). The local density approximation limit of the momentum density and the Compton profiles of Al. *J. Phys.-Condens. Mat.*, 16, 7363–7378.
18. Bross, H. (2005). Electronic structure of Li with emphasis on the momentum density and the Compton profile. *Phys. Rev. B*, 72, 115109(14 pp.).
19. Chu-Nan, Chang, Yu-Mei, Shu, Chuhn-Chuh, Chen, & Huey-Fen, Liu. (1993). The Compton profiles of tantalum. *J. Phys.-Condens. Mat.*, 5, 5371–5376.
20. Joshi, K. B., Pandya, R. K., Kothari, R. K., & Sharma, B. K. (2009). Electronic structure of AlAs: A Compton profile study. *Phys. Status Solidi B*, 246, 1268–1274.
21. Ohata, T., Itou, M., Matsumoto, I., Sakurai, Y., Kawata, H., Shiotani, N., Kaprzyk, S., Mijnders, P. E., & Bansil, A. (2000). High-resolution Compton scattering study of the electron momentum density in Al. *Phys. Rev. B*, 62, 16528–16535.
22. Sharma, G., Joshi, K. B., Mishra, M. C., Kothari, R. K., Sharma, Y. C., Vyas, V., & Sharma, B. K. (2009). Electronic structure of AlAs: A Compton profile study. *J. Alloys Compd.*, 485, 682–686.
23. Kawasuso, A., Maekawa, M., Fukaya, Y., Yabuuchi, A., & Mochizuki, I. (2011). Polarized positron annihilation measurements of polycrystalline Fe, Co, Ni, and Gd based on Doppler broadening of annihilation radiation. *Phys. Rev. B*, 83, 0406(R).
24. Kontrym-Sznajd, G. (2013). Utilization of symmetry of solids in experimental investigations. *Nukleonika*, 58, 205–208.
25. Waspe, R. L., & West, R. N. (1982). The Fermi surface of gadolinium. In P. G. Coleman, S. C. Sharma, & L. M. Diana (Eds.), *Positron annihilation* (pp. 328–330). Amsterdam: North-Holland Publ. Co.
26. Kontrym-Sznajd, G., & Samsel-Czekala, M. (2012). Special directions in momentum space. II. Hexagonal, tetragonal and trigonal symmetries. *J. Appl. Crystal.*, 45, 1254–1260.
27. Kontrym-Sznajd, G., Samsel-Czekala, M., Pietraszko, A., Sormann, H., Manninen, S., Huotari, S., Hämäläinen, K., Laukkanen, J., West, R. N., & Schülke, W. (2002). Electron momentum density in yttrium. *Phys. Rev. B*, 66, 155110(10 pp).
28. Walters, P. A., Mayers, J., & West, R. N. (1982). Two-dimensional electron-positron momentum densities in the hcp metals: Mg, Zn, and Cd. In P. G. Coleman, S. C. Sharma, & L. M. Diana (Eds.), *Positron annihilation* (pp. 334–336). Amsterdam: North-Holland Publ. Co.
29. Stewart, A. T. (1957). Momentum distribution of metallic electrons by positron annihilation. *Can. J. Phys.*, 35, 168–183.
30. Lam, L., & Platzman, P. M. (1974). Momentum density and Compton profile of the inhomogeneous interacting electronic system. I. Formalism. *Phys. Rev. B*, 9, 5122–5127.
31. Kubo, Y. (2005). Electron correlation effects on Compton profiles of copper in the GW approximation. *J. Phys. Chem. Solids*, 66, 2202–2206.
32. Bansil, A. (1975). Special directions in the Brillouin zone. *Solid State Commun.*, 16, 885–889.
33. Fehlnner, W. R., Nickerson, S. B., & Vosko, S. H. (1976). Cubic harmonic expansions using Gauss integration formulas. *Solid State Commun.*, 19, 83–86.
34. Fehlnner, W. R., & Vosko, S. H. (1976). A product representation for cubic harmonics and special directions for the determination of the Fermi surface and related properties. *Can. J. Phys.*, 54, 215–216.
35. Wasserman, E., Stixrude, L., & Cohen, R. E. (1996). Thermal properties of iron at high pressures and temperatures. *Phys. Rev. B*, 53, 8296–8309.